Supramolecular Assembly of Gelatin and Inorganic Polyanions: Fine-Tuning the Mechanical Properties of Nanocomposites by Varying Their Composition and Microstructure

Imane Baroudi,[†] Corine Simonnet-Jégat,[†] Catherine Roch-Marchal,[†] Nathalie Leclerc-Laronze,[†] Carine Livage,[†] Charlotte Martineau,[†] Christel Gervais,[▽] Emmanuel Cadot,[†] Florent Carn,[‡] Bruno Fayolle,[§] and Nathalie Steunou*[,†,▽]

[†]Institut Lavoisier, UMR CNRS 8180, Université de Versailles-Saint-Quentin-en-Yvelines (UVSQ), 45 avenue des Etats-Unis, 78035 Versailles Cedex, France

[‡]Laboratoire Matière et Systèmes Complexes (MSC), UMR CNRS 7057, Université Paris Diderot, Bât. Condorcet, 10 rue A. Domon et L. Duquet, 75013 Paris, France

[§]Procédés et Ingénierie en Mécanique et Matériaux, UMR CNRS 8006, ENSAM, 151 Bld de l'Hôpital, 75013 Paris, France

[▽]UPMC Univ Paris 06, UMR 7574, Chimie de la Matière Condensée de Paris, and [#]CNRS, UMR 7574, Chimie de la Matière Condensée de Paris, Collège de France, 11 place Marcelin Berthelot, 75231 Paris Cedex 05, France

ABSTRACT: A series of bionanocomposites has been synthesized through a complex coacervation process inducing the assembly of gelatin with a wide range of inorganic polyanions (IPyAs) differing by their diameter and charge and including polyoxometalates (POMs) and a polythiomolybdate cluster. The microstructure and stoichiometry of these hybrid coacervates, which are strongly dependent on the charge matching between both components, have been studied by combining Fourier transform infrared (FT-IR) spectroscopy, solid-state nuclear magnetic resonance (NMR), thermogravimetric analysis (TGA), elemental analysis, differential scanning calorimetry (DSC), scanning electron microscopy (SEM), and energy-dispersive X-ray (EDX) elemental mapping. The mechanical properties of these materials were deeply characterized by tensile measurements at large deformation, revealing different behaviors (i.e., elastomer and ductile), depending on the nature of the IPyA. It is noteworthy that the mechanical properties of these bionanocomposites are strongly enhanced, compared to pure gelatin hydrogels. When attempting to connect structure and properties in these bionanocomposites, we have demonstrated that the density of cross-links (gelatin triple helices and IPyA) is the key parameter to control the extensibility of these materials.

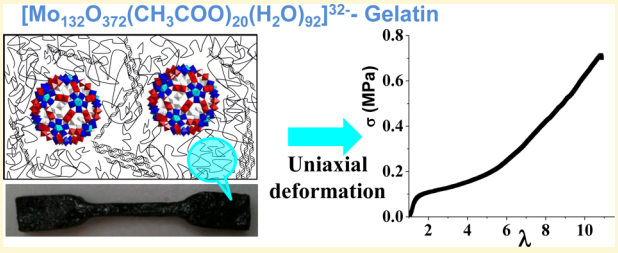

INTRODUCTION

Biopolymer-based materials have recently received increasing attention, since petroleum-based polymer materials have led to serious economical and environmental concerns, as a result of the increasing high oil price, as well as the nondegradable and nonrenewable nature of synthetic polymers.[1,2] Because of their unique high elasticity, elastomers are very attractive materials and have found a wide range of applications in industry, national defense, cutting-edge technology, and our daily life.[3−7] Bioelastomers with potential use in tissue engineering, drug delivery, and *in vivo* sensing have been recently reported,[4,8−13] but the development of potential applications generally requires their reinforcement by appropriate fillers that enhance the physical properties, such as hardness, Young's modulus, tensile strength, and abrasion resistance.[6,7,14−19]

Gelatin is a protein biopolymer derived from hydrolysis of collagenous tissues. Because of its low cost, biodegradability, nontoxicity and renewability, gelatin is currently used in the field of microencapsulation and is suitable for the elaboration of new environmentally friendly materials (drug carriers, tissue scaffolds).[20−24] However, the poor mechanical properties and thermal stability of gelatin, as well as its high water solubility, largely limit its application. Therefore, in the last decades, gelatin has been combined with a large range of plasticizing agents (glycerol, D-sorbitol, ethylene glycol, etc.)[25−27] or reinforcing species, including polymers (poly(vinyl alcohol), chitosan),[28−31] carbon nanotubes,[32,33] or inorganic entities (silica, hydroxyapatite, clay minerals, etc.);[20−24,34−40] the resulting composites present significant improvements in different aspects, with regard to cell proliferation, biodegradation, porosity, and mechanical properties.

Received: July 16, 2014
Revised: January 20, 2015
Published: January 27, 2015

According to IUPAC, coacervation is related to a "separation into two liquid phases in colloidal systems. The phase more concentrated in colloid component is the coacervate, and the other phase is the equilibrium solution". In the past few years, a widespread interest has been devoted to this soft-matter phenomenon, because of the possibility of processing complex fluids for microencapsulation and protein purification, in domains such as pharmacy or cosmetics.[41−46] The phenomenon, which is generally based on electrostatic interactions between protein and polyelectrolytes or between two polyelectrolytes bearing opposite charges, is divided into: "simple" and "complex" coacervation. While simple coacervation usually involves a single type of colloids, complex coacervation is observed for systems that contain at least two types of colloids. More recently, this phase separation process has also been used in the field of materials science for the preparation of hydrogels and biohybrid inorganic−organic materials involving organic polyelectrolytes/(bio)polymers and different inorganic solids (iron oxide, silica, clay minerals, quantum dots, etc.).[24,47−52] Until recently, polyoxometalates (POMs), which are discrete metal-oxo clusters of well-defined symmetry and molecular structure,[53−57] with several potential applications in catalysis and biomedicine, have been rarely combined with polycations and biopolymers,[58−67] despite the fact that the interactions between these components may lead to complementary and synergetic properties. In this context, we have previously reported that the electrostatic interactions between decavanadate anionic clusters ($[H_2V_{10}O_{28}]^{4-}$) and positively charged gelatin chains represent the major driving force for the formation of ion-pair aggregates.[68] By controlling the physicochemical parameters of this system (concentrations of precursors, pH, temperature, ionic strength), a phase diagram has been established, showing a two-step liquid−liquid phase separation in fair agreement with a complex coacervation process.[68] The characterization of semidilute gelatin−decavanadate solutions by combining microcalorimetry and rheology has evidenced the temperature-dependent role of decavanadates on the rheological properties and transition of conformation of gelatin: at $T > 27$ °C, decavanadates exert the role of physical cross-linkers and can favor the nucleation of a few gelatin triple helices, whereas, at $T < 27$ °C, the decavanadates do not affect the formation of an extended network of triples helices but certainly improve their thermal stabilization.[69] In another study, we have taken advantage of this complex coacervation process to prepare a new type of hybrid hydrogel in which the weak mechanical properties of gelatin hydrogels are converted to a striking rubber-like behavior.[70]

In the present work, we have extended the synthesis of hybrid coacervates to a wide family of inorganic polyanions, including a thiomolybdate cluster with a cubane-type Mo_3S_4 topology[71,72] and POMs[73−78] (see Scheme 1, as well as Figures S1−S3 in the Supporting Information (SI)). This study is focused on addressing the following questions:

(i) Is this coacervation process tunable to inorganic polyanions of different charge and nuclearity?

(ii) Is it possible to reinforce and modulate the mechanical properties of gelatin hydrogels by selecting the appropriate IPyA as inorganic filler and, in this way, finely tuning the microstructure and composition of hybrid coacervates?

Scheme 1. Molecular Structures of Inorganic Polyanions: (a) $[Mo_3S_4(Hnta)_3]^{2-}$,[79] (b) $[SiW_{12}O_{40}]^{4-}$ and $[BW_{12}O_{40}]^{5-}$,[73] (c) $[PW_{11}O_{39}]^{7-}$,[74,75] (d) $[H_7P_8W_{48}O_{184}]^{33-}$,[78] and (e) $[Mo_{132}O_{372}(CH_3COO)_{30}(H_2O)_{72}]^{42-}$,[80] [a]

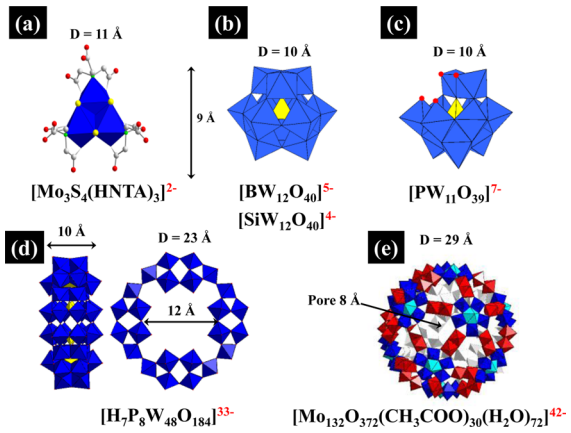

[a] MO_6 (with M = W or Mo) are represented by blue octahedra. For panel (a), the white, red, yellow and green spheres correspond to C, O, S, and N atoms, respectively. For panels (b) and (c), XO_4 (X = B, Si or P) are represented by yellow tetrahedra. For panel (e), dimers of Mo^VO_6 are represented by red octahedra, while $Mo^{VI}O_7$ and $Mo^{VI}O_6$ of pentagonal units are depicted in blue (see the SI for the complete description of the structures).

One critical issue of this study concerns the chemical and thermodynamic compatibility between gelatin and IPyA that governs the dispersion and aggregation of nanofillers. Actually, the enhancement of mechanical properties is strongly dependent on the interfacial properties between the inorganic filler and polymer that drive both the polymer microstructure (degree of crystallinity, cross-link/entanglement density, confinement effect, etc.) and the interactions between both components (irreversible or reversible bonds formation, interfacial slip, etc.).

EXPERIMENTAL SECTION

Chemicals. Commercial gelatin extracted from porcine skin (Type A with a bloom of ∼175 g), corresponding to an average molecular weight of ∼40000 g mol^{-1} and an isoelectric point (IEP) of ∼8 (according to the supplier) was purchased from Sigma−Aldrich.

Synthesis of Inorganic Polyanions (IPyA). The Keggin-type potassium salts $K_5[BW_{12}O_{40}]\cdot 11H_2O$, $K_7[PW_{11}O_{39}]\cdot 14H_2O$, $K_4[SiW_{12}O_{40}]\cdot 5H_2O$ (see Scheme 1 and Figure S1 in the SI) have been synthesized according to previous publications[73−75] and characterized by FT-IR (see Figure S4 and Table 1 in the SI) and/or NMR spectroscopy (see Figures S5 and S9 in the SI). A decavanadate solution of $[H_2V_{10}O_{28}]^{4-}$ was prepared by using a proton exchange resin, as previously reported.[76,77] The salt $K_{28}Li_5H_7[P_8W_{48}O_{184}]\cdot 92H_2O$ prepared in three steps, as previously described by Contant and Teze,[78] was checked via FT-IR (Figure S4 and Table 1 in the SI), ^{31}P NMR in solution (Figure S6 in the SI) and ^{31}P MAS NMR spectroscopy (Figures S9−S11 in the SI). The thiomolybdate-based salt $Na_2[Mo_3S_4(HNTA)_3]\cdot 7H_2O$ (where HNTA = $[N(CH_2COO)_2(CH_2COOH)]^{2-}$) and Keplerate-type molybdate salt $(NH_4)_{42}[Mo_{132}O_{372}(CH_3COO)_{30}(H_2O)_{72}]\cdot 300H_2O$, ca.$10CH_3COONH_4$, have been prepared according to already published procedures[79,80] and characterized by FT-IR spectroscopy and ^1H NMR in solution (see Figures S4 and S7, as well as Table 1, in the SI).

Preparation of IPyA Solutions. Inorganic polyanion (IPyA) solutions of the desired concentration were obtained by dissolution of the required quantity of compound in aqueous solution. The pH was then adjusted to 3, using an aqueous HCl solution (2 M). The stability

of the different IPyA at pH 3 is evaluated by recording solution NMR spectroscopy (see Figures S5−S7, as well as Table 2, in the SI).

Preparation of Gelatin Solutions. Gelatin solutions (10 wt %, 2.5 mM) were prepared by swelling the gelatin granules in an aqueous solution for a minimum period of 3 h at a temperature of 5 °C. Gelatin was then dissolved at a temperature of 50 °C, using a magnetic stirrer for 30 min at 300 rpm.

Preparation of IPyA−Gelatin Coacervates. When gelatin is dissolved, the pH is adjusted to pH 3 with an aqueous HCl solution (2 M) and the temperature is fixed at 40 °C. The progressive addition of 200 mL of the IPyA solutions at different concentrations (see Table 3 in the SI) to 100 mL of the gelatin solution then gives rise to an immediate phase separation. The as-prepared biphasic coacervates are finally aged for 20 min at 40 °C before performing the different characterizations (see Figures S8−S15 in the SI).

Characterization of IPyAs in Solution. ^{1}H and ^{31}P NMR spectra of the IPyAs solutions were recorded at 298 K on Bruker Avance 200 or Avance 300 NMR spectrometers. ^{31}P chemical shifts were referenced to a 85 wt % H_3PO_4 solution ($\delta(^{31}P) = 0$ ppm).

Characterization of IPyA Salts and IPyA-G Coacervates. Elemental analyses were performed by the Service Central d'Analyze of CNRS−Institut des Sciences Analytiques (Villeurbane, France). Thermogravimetric analysis (TGA) was performed on a TGA apparatus (Perkins−Elmer, Model SDA 6000). Solids were heated up to 600 °C with a heating rate of 5 °C min^{-1} in an oxygen atmosphere. Infrared spectra were recorded on a FTIR Magna 550 Nicolet spectrophotometer using the technique of pressed KBr pellets at a resolution of 4 cm^{-1}. The single-pulse (90° pulse length = 2.9 μs) ^{31}P MAS (10 kHz) NMR spectra were recorded on a Bruker Avance 500 spectrometer (B_0 = 11.7 T, Larmor frequencies of 500.1 and 202.2 MHz for ^{1}H and ^{31}P, respectively) using a 3.2 mm probe. The recycle delays were set to 100 s to ensure full return of the ^{31}P magnetization to equilibrium and 300−600 transients were accumulated per sample. ^{1}H 64-step small-phase incremental alternation (SPINAL-64)[81] decoupling was applied during acquisition (70 kHz RF field). ^{31}P chemical shifts were referenced to H_3PO_4 at 0 ppm. The NMR spectra were analyzed using the Dmfit software.[82] A double-quantum single-quantum (DQ-SQ) ^{31}P−^{31}P MAS (10 kHz) NMR spectrum of $K_{28}Li_5[H_7P_8W_{48}O_{184}]\cdot 92H_2O$ was acquired with a recoupling sequence POST-C7[83]. The excitation/reconversion duration was optimized to 1.2 ms, with a radio frequency (RF) field of ∼70 kHz. ^{1}H SPINAL-64 decoupling was applied during the excitation/reconversion and signal acquisition periods. Eighty (80) t1 slices with 32 transients each were coadded. Phase-sensitive detection in the indirect dimension was performed using the States method.[84] ^{11}B MAS NMR spectra were recorded at 11.75 T on a Bruker Avance 500 wide-bore spectrometer operating at 128.28 MHz, using a Bruker 4-mm probe and a spinning frequency of the rotor of 14 kHz. The spectra were acquired using a spin−echo $\theta-\tau-2\theta$ pulse sequence with $\theta = 90°$ to overcome problems of probe signal. The τ delay was synchronized with the spinning frequency and a recycle delay of 1 s was used. Chemical shifts were referenced to $BF_3(OEt)_2$ (δ = 0 ppm). SEM images have been recorded on a JEOL Model JSM-7001F microscope using gold-coated samples equipped with an energy-dispersive X-ray (EDX) spectrometer and a X-Max SDD (silicon drift detector) by Oxford. The EDX spectra were acquired with a voltage acceleration of 15 kV, an acquisition time of 120 s, and >10 000 counts. All coacervates were analyzed via differential scanning calorimetry (DSC) running in conventional mode, using a Mettler Toledo DSC1 setup. Hydrated coacervates were extracted from the biphasic mixture 2 min after their formation and deposited on paper. Pieces of coacervates with a typical mass of ∼20 mg were stamped out of the coacervates and sealed in 40-mL aluminum pans with a perforated lid. The reference was an empty pan and the heat exchange was calibrated with indium (T_m = 156.5 °C, ΔH_m = 28.68 J g^{-1}). The thermal protocol was identical for all samples: samples were introduced at room temperature, and equilibrated 2 min at 25 °C before starting the heating ramp up to 200 °C at a rate of 10 °C min^{-1}. The enthalpy associated with the endothermic transition was calculated as the area of the endothermic peak with a linear baseline far from the onset and endset temperatures.

Formulation of the Coacervate Tablets. After macroscopic phase separation, the simple and complex coacervates were heated with their supernatant solution at 70 °C for 15 min and then 90 °C for 5 min before being poured without their supernatant solution into rectangular molds (length = 6 cm, width = 9 cm) thermalized at 70 °C. In order to avoid the formation of a brittle surface due to drying, which could not be reversibly reswollen, the molds are immediately capped in an almost hermetic manner. Rubbery coacervate "thick" tablets were finally formed by cooling at room temperature for 15 min and then kept at 2 °C for 1 day.

Tensile Test Measurements. In order to perform tensile measurements at a given relative weight loss of solvent, the drying kinetic of the nanocomposite samples was measured under the experimental conditions (see Figure S16 in the SI) used for the mechanical test at a temperature (T) of 23 °C and a humidity rate (HR) of 54%. The mechanical investigations have been mainly performed on "wet" samples displaying a relative weight loss of 0.01. Nevertheless, some measurements have been performed at larger $\Delta m/m_0$ values in order to characterize the evolution of the sample mechanical behavior during drying. The mechanical tests were carried out on a tensile testing machine (Instron, Model 4302), using a 0.1 kN load cell. The instrument resided in a temperature- and humidity-rate-controlled room with T = 23 °C and HR = 54%. Dumbbell-shaped specimens (Figure 1b−d), having a calibrated length of 15 mm and a width of 2 mm, were cut from the films with an MTS H4 stamp. These samples were held on the machine between pneumatic clamps altered with wood strips to better grip the rubbery materials. It is worth noting that gelatin hydrogels with gelatin concentrations up to 15 wt % simply prepared through dissolution broke systematically into the clamps during the clamp tightening. Tensile measurements were performed at a constant crosshead displacement rate of 100 mm min^{-1}. Cyclic tests were performed according to a four-step trial composed of an initial loading ramp performed at a constant crosshead displacement rate of 100 mm min^{-1}, up to a maximum drawing ratio (λ_{max}), followed by an unloading ramp at a constant crosshead displacement rate of 100 mm min^{-1} and finally by a loading ramp performed at the same displacement rate up to failure. When failure occurs, the corresponding stress and stretch will give access to stress at break (σ_{break}) and lambda at break (λ_{break}), respectively.

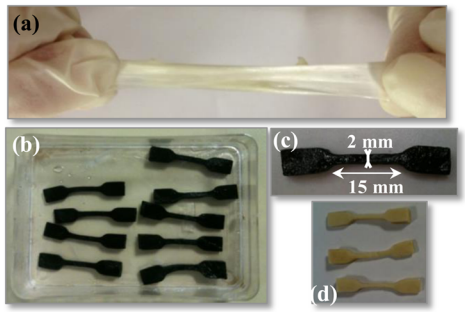

Figure 1. Photograph of (a) G-[BW_{12}] coacervate under stretching. Panels (b)−(d) show dumbbell-shaped specimens of (b, c) G-[Mo_{132}] and (d) G-[P_8W_{48}], having a calibrated length of 15 mm and a width of 2 mm.

RESULTS AND DISCUSSION

Stability of IPyAs under Conditions of Low Concentrations and pH 3. In order to prepare bionanocomposites between gelatin and IPyAs, the first step consists of determining a pH domain where the inorganic anions and gelatin are stable and may interact by electrostatic interactions. In acidic solution, gelatin macromolecules are in a random coil conformation with fully protonated amine (pK_a(R-NH_3^+/R-

Table 1. Summary of the Main Results of Experiments Performed on IPyA−Gelatin Coacervates

hybrid	IPyAs	$\mathbf{R}^a$	$\mathbf{X}^b$	λ_{break}	mechanical behavior
G-[Mo_3S_4]	$[Mo_3S_4(HNTA)_2(NTA)]^{3-}$	0.3	12	6.8	elastomer
G-[V_{10}]	$[H_2V_{10}O_{28}]^{4-}$	0.39	16	8.0	elastomer
G-[BW_{12}]	$[BW_{12}O_{40}]^{5-}$	0.64	9	10.6	ductile (S-shape)
G-[PW_{11}]	$[HPW_{11}O_{39}]^{6-}$	0.57	8.5	7.3	elastomer
G-[SiW_{12}]	$[SiW_{12}O_{40}]^{4-}$	0.65	9	12	ductile (plastic)
G-[P_8W_{48}]	$[H_{16}P_8W_{48}O_{184}]^{24-}$	0.81	2.5	11	ductile (S-shape)
G-[Mo_{132}]	$[Mo_{132}O_{372}(CH_3COO)_{20}(H_2O)_{92}]^{32-}$	0.55	1.12	11.5	ductile (plastic)

[a]Weight ratio: $\mathbf{R}$ = wt $\%_{IPyA}$/wt $\%_G$. [b]Molar ratio: $\mathbf{X} = n_{IPyA}/n_G$.

NH_2) ≈ 10.5) and carboxylic acid functions (pK_a(R-COOH/R-COO^-) ≈ 4), giving rise to a global positive charge (pI ≈ 8). Thus, gelatin behaves like a weak cationic polyelectrolyte below pH 8. Therefore, attractive electrostatic interactions between IPyAs and gelatin may be expected at pH <4. Our previous work on the coacervation process between $[H_2V_{10}O_{28}]^{4-}$ and gelatin has clearly shown the suppression of any interactions at pH ≥4.5, which is certainly due to the deprotonation of carboxylic acid functions of gelatin and, thus, to a decrease of the global positive charge of gelatin.[68] Moreover, since polyoxometalates are labile molecular clusters that are sensitive toward hydrolysis, especially in diluted aqueous solutions, it was of primary importance to ascertain that IPyAs are stable at low concentration (typically 0.5 mM) and pH 3 before mixing the IPyAs with gelatin. The stability of IPyAs under those physicochemical conditions has thus been studied by recording the solution NMR spectroscopy. As reported previously, solutions of $[BW_{12}O_{40}]^{5-}$ and $[SiW_{12}O_{40}]^{4-}$ at 0.5 mM are stable at pH 3.[85,86] $[PW_{11}O_{39}]^{7-}$ and $[H_7P_8W_{48}O_{184}]^{33-}$ are known to be stable in quite a large pH domain (i.e., typically between pH 1 and pH 8 for $[H_7P_8W_{48}O_{184}]^{33-}$).[78,87] However, their protonation state varies significantly with pH and has been determined by ^{31}P NMR spectroscopy in solution (see Figures S5 and S6, as well as Table 2, in the SI). As a consequence, both POMs are present in solution at pH 3, as $[HPW_{11}O_{39}]^{6-}$ and $[H_{16}P_8W_{48}O_{184}]^{24-}$. As already reported,[79,88] $[Mo_3S_4(Hnta)_3]^{2-}$ is stable over a wide range of pH (from 1 to 10). Following the same strategy, the ^{1}H NMR spectrum of $[Mo_{132}O_{372}(CH_3COO)_{30}(H_2O)_{72}]^{42-}$ at pH 3 (Figure S7 in the SI) clearly shows the decrease of coordinated acetate ligands upon decreasing pH, which is consistent with the molecular formula $[Mo_{132}O_{372}(CH_3COO)_{20}(H_2O)_{92}]^{32-}$ (see the SI for more details).

Synthesis of IPyA−Gelatin Hybrids. Inorganic polyanions (IPyAs)−gelatin hybrids have been synthesized by mixing a solution of IPyA at different concentrations (see Table 3 in the SI) and a 2.5 mM gelatin solution at pH 3. The experiments have been performed at 40 °C, because of the thermoreversible property of gelatin: above the temperature of gelification (T_{gel} ≈ 27 °C for a mammalian gelatin), gelatin chains are soluble in water and exhibit a random coil configuration; at temperatures below T_{gel}, they form reversible physical gels. The IPyA−gelatin bionanocomposites were obtained for large [M]/[G] ratios (typically 36 < [M]/[G] < 120, with [M] and [G] being equal to the molar concentrations of metal cation (Mo, W, or V) and gelatin, respectively; see Table 3 in the SI), for which the addition of IPyA solutions to the gelatin sol gives rise to a phase separation between viscous phases and transparent solutions (see Figure S13 in the SI). These viscous phases have been extracted from the supernatant solutions and characterized. In the wet state and at room temperature, they present very interesting mechanical properties, namely, a striking high deformation upon stretching (see Figures 1a, as well as Figures S13d and S13e in the Supporting Information), as previously reported for the decavanadate−gelatin hybrid.[70] Thus, these phases may be easily processed in various forms, including coatings, membranes, monoliths, and fibers. Upon drying, all these viscous phases evolve to glassy compounds, because of the vitreous transition of gelatin. A summary of the IPyA-G coacervates and their physicochemical properties is given in Table 1 in the current paper.

Characterization of IPyA−Gelatin Hybrids. The IPyA−gelatin coacervates were characterized by FT-IR spectroscopy, with comparison to the parental gelatin and IPyAs (see Figure S4 in the SI). The main vibrations bands of all these compounds are provided in Table 1 in the SI. The FT-IR spectra of IPyA−gelatin hybrids present the characteristic vibrations bands of gelatin and IPyA. The FT-IR spectrum of G-[Mo_3S_4] presents the characteristic vibrations bands of $[Mo_3S_4(Hnta)_3]^{2-}$ at 923, 956, 997, and 784 cm^{-1}. For coacervates with Keggin-type ions (i.e., G-[BW_{12}], G-[PW_{11}], G-[SiW_{12}]), as well as G-[P_8W_{48}] and G-[Mo_{132}], the IPyAs are clearly identified in the gelatin matrix by the vibration bands of the metal-oxide skeleton between 700 cm^{-1} and 1100 cm^{-1} (see Table 1 in the SI), despite the fact that their position is weakly shifted, compared to the parent polyoxometalate. This result can be interpreted by a modification of the IPyAs environment, as a result of interactions with amino groups of gelatin. With regard to gelatin, the vibration band at 1648 cm^{-1} that can be assigned to the amide I group is systematically present in the IR spectra of gelatin−IPyA hybrids. The vibration bands typical of the amino and carboxylate groups of amino acids are also present (ν(COO) ≈ 1400 cm^{-1}) (see Table 1 in the SI).

Solid-State NMR. The IPyA−gelatin coacervates were also characterized by solid-state NMR. As already recently reported on a similar G-[BW_{12}] coacervate,[85] the ^{11}B MAS NMR spectrum of G-[BW_{12}] hybrid indicates that the polyanion is immobilized in the gelatin matrix without alteration of its molecular structure (see Figure S8 in the SI). Figure S9 in the SI shows the ^{31}P MAS NMR spectra of the G-[PW_{11}] and G-[P_8W_{48}] coacervates and the parent POM. The spectrum of $K_7[PW_{11}O_{39}]\cdot 14H_2O$ (Figure S9a in the SI) presents one signal at −10.7 ppm, in fair agreement with the ^{31}P NMR spectrum in solution (Figure S5 in the SI). In contrast, the ^{31}P MAS NMR spectrum of G-[PW_{11}] with three signals is more complex: a first signal at −10.5 ppm ($\Delta\nu_{1/2}$ = 200 Hz), which can be assigned to the $[HPW_{11}O_{39}]^{6-}$ polyanion; a sharp line at −15.4 ppm ($\Delta\nu_{1/2}$ = 65 Hz), whose chemical shift and line width are characteristic of $[PW_{12}O_{40}]^{3-}$;[89] and a third broad signal at −12.0 ppm ($\Delta\nu_{1/2}$ = 250 Hz). This last broad signal may result from a distribution of chemical shifts and therefore of various

Table 2. (a) Molecular Formula and (b) Chemical Composition of IPyA–Gelatin Hybrids Determined by Thermogravimetric Analysis (TGA) and Elemental Analyses after Drying the Samples at Room Temperature (RT) for 24 h

(a) Molecular Formula of IPyA–Gelatin Hybrids

hybrid	molecular formula	M_w[a] (g mol^{-1})
G-[Mo_3S_4]	$[Mo_3S_4(HNTA)_2(NTA)]_{12}$·G·6NaCl·350$H_2O$	58 435
G-[V_{10}]	$Na_{28}[H_2V_{10}O_{28}]_{16}$·G·466$H_2O$	64 392
G-[BW_{12}]	$K_9[BW_{12}O_{40}]_9$·G·400H_2O	73 272
G-[PW_{11}]	$K_{12}Na_3[HPW_{11}O_{39}]_{8.5}$·G·400$H_2O$	70 503
G-[SiW_{12}]	$[SiW_{12}O_{40}]_9$·G·400H_2O	73 066
G-[P_8W_{48}]	$[K_{6.5}Li_{3.1}H_{16}P_8W_{48}O_{184}]_{2.5}$·G·67.25LiCl·550$H_2O$	83 533
G-[Mo_{132}]	$[Mo_{132}O_{372}(CH_3COO)_{20}(H_2O)_{92}]_{1.12}$·G·297$H_2O$	69 382

(b) Chemical Composition of IPyA–Gelatin Hybrids

	Chemical Composition (wt %)							
hybrid	IPyA	gelatin	H_2O	ions	**R**[b]	**X**[c]	n^-/n^+[d]	ΔH_{endo} (J/g) (hy/dr)[e]
G-[Mo_3S_4]	20.3	68.4	10.7	0.6	0.3	12	1	1124/1223
G-[V_{10}]	24	62	13	1.0	0.39	16	1.78	
G-[BW_{12}]	35.1	54.6	9.8	0.46	0.64	9	1.25	126/620
G-[PW_{11}]	32	57	10	0.76	0.57	8.5	1.42	136/685
G-[SiW_{12}]	35.4	54.7	13.1	0	0.65	9	1	166/544
G-[P_8W_{48}]	38.9	47.9	11.9	1.4	0.81	2.5	1.67	135/627
G-[Mo_{132}]	32.0	57.7	10.4	0	0.55	1.12	1	297/776

[a] M_w = molecular weight. [b] Weight ratio: **R** = wt $\%_{IPyA}$/wt $\%_G$. [c] Molar ratio: **X** = n_{IPyA}/n_G. [d] Molar charge ratio. [e] Melting enthalpy determined by DSC experiments, based on values from hydrated and dried samples.

chemical environments around the P atoms of the POM encapsulated within the gelatin hydrogel. Moreover, according to the shift of this signal toward high field, compared to that of $K_7[PW_{11}O_{39}]\cdot 14H_2O$, the local environment of this POM is notably different in both compounds (i.e., $K_7[PW_{11}O_{39}]\cdot 14H_2O$ and G-[PW_{11}]), as a result of its confinement in the gelatin matrix. Moreover, electrostatic interactions or hydrogen bonds between this POM and amino groups of gelatin may occur, since the detection of the $[PW_{12}O_{40}]^{3-}$ species by ^{31}P MAS NMR supports a conversion of $[HPW_{11}O_{39}]^{6-}$ into $[PW_{12}O_{40}]^{3-}$ to produce necessarily other phosphotungstates of different nuclearity. However, considering the FT-IR spectrum of G-[PW_{11}] for which the most intense vibration bands of the metal oxide skeleton correspond to the lacunary $[HPW_{11}O_{39}]^{6-}$ (*vide supra*) species and the relative intensity (~80%) of the line at −12 ppm, we can presume that this POM is the main inorganic filler embedded in the gelatin matrix. The $^{31}P-^{31}P$ two-dimensional NMR spectrum (see Figure S11a in the SI) of the salt $K_{28}Li_5[H_7P_8W_{48}O_{184}]\cdot 92H_2O$ presents four isotropic signals at −6.9, −7.4, −7.7, and −7.8 ppm (see the SI for the full interpretation of this 2D NMR experiment). The ^{31}P MAS NMR spectrum of G-[P_8W_{48}] (Figure S9b in the SI) displays one broad signal, centered at approximately −6.8 ppm, which is fully consistent with that of the polyanion at pH 3 (see Figure S7 in the SI), confirming the retention of its integrity in the gelatin hydrogel under the protonated form of $[H_{16}P_8W_{48}O_{184}]^{24-}$. The lack of spectral resolution giving rise to a single resonance is certainly due to a distribution of chemical shifts, as a result of a distribution of the environments of $[H_{16}P_8W_{48}O_{184}]^{24-}$, as observed for G-[$PW_{11}$].

For the G-[BW_{12}], G-[PW_{11}], and G-[P_8W_{48}] coacervates, similar MAS NMR spectra were obtained by varying the initial POM concentration or after drying the samples for ~1 h at RT (see Figures S8–S10 in the SI). Therefore, the composition of these coacervates seems to be fully independent of the initial amount of POM and gelatin and the molar POM/G ratio. Moreover, the chemical environment of the POMs in the gelatin matrix and the interface between both components are presumably equivalent in these coacervates.

Fine Tuning the Chemical Composition of Coacervates by the Nature of IPyA. The chemical composition of the IPyA–gelatin coacervates were determined by combining elemental and TGA analyses on freshly prepared samples (see Table 5 in the SI) and samples aged for ~24 h (see Table 2 in the current work, as well as Table 4 in the SI). The water content of the samples was mainly determined by TGA. For each IPyA–gelatin coacervate, three different samples were prepared, under the same synthesis conditions, and their chemical compositions, as determined by coupling TGA and elemental analyses, are similar. The chemical composition of IPyA–gelatin coacervates given in Table 2 in the current work and Table 4 in the SI is the average of that of the three samples. First, the chemical composition $(CH_{1.56}O_{0.42}N_{0.31})_{1625}$ of gelatin has been established by elemental analysis and considering the water content (~10 wt %) measured by TGA. The chemical formula of coacervates could be determined by taking into account the protonation state of the IPyAs at pH 3 previously determined by NMR spectroscopy in solution (*vide supra*), the charge of a gelatin chain, and the contents of counterions given by the elemental analyses. Considering that the positive charges of gelatin are mainly given by arginine and lysine amino acids, we have previously estimated that 9 of every 100 residues of gelatin are positively charged at pH 3, giving the average molecular charge of G^{36+}.[61] Following this strategy, the chemical formula and molecular weight of coacervates (Table 2a) could be established and the weight ratio **R** (which is defined as **R** = wt $\%_{IPyA}$/wt $\%_G$), the molar ratio **X** (which can be defined as **X** = n_{IPyA}/n_G), and the molar charge ratio (given as n^-/n^+) of these coacervates could be calculated accordingly (see Table 2b in the current work). The parameters n^- and n^+ correspond to the respective molar quantities of negative and positive charges provided by IPyA and gelatin. For G-[Mo_3S_4], it is worth noting that the charge of the thiomolybdate cluster could be deduced from the chemical composition and the

content of Na^+ and Cl^- anions, since the electroneutrality of the solid requires that the thiomolybdate cluster bears a charge of −3. Therefore, this complex is encapsulated in the gelatin matrix in the form of $[Mo_3S_4(HNTA)_2(NTA)]^{3-}$. The deprotonation of one of the HNTA ligands at pH 3 is in agreement with the preparation of the G-$[Mo_3S_4]$ coacervate, which requires an alcalinization step of the initial $[Mo_3S_4(HNTA)_3]^{2-}$ solution. It is worth noting that the amount of IPyA and gelatin in these coacervates is completely independent of the concentrations and molar ratio of the initial IPyA and gelatin solutions, showing that these hybrid materials present a well-defined stoichiometry, as previously reported for the G-$[V_{10}]$ coacervate.[70]

However, the content of coacervate counterions is strongly dependent on the physicochemical conditions used for the synthesis of IPyAs and coacervates. As an example, the high salt content of G-$[P_8W_{48}]$ is certainly strongly related to the high amount of LiCl used to synthesize the POM.[78] Interestingly, one can notice that the freshly prepared coacervates present a high hydration rate (wt %(H_2O) ≈ 40−45 wt %), which is comparable for all compounds (see Table 5 in the SI) and decreases for most compounds to ∼10−13 wt % for ∼24 h (see Table 2 in the current paper). The decrease of the molar ratio **X** (**X** = n_{IPyA}/n_G), as a function of the charge of IPyA depicted in Figure 2a, clearly shows that the charge of IPyA is the key chemical parameter to finely tune the polyanion content of the coacervates. This molar ratio **X** evolves from 16 for G-$[V_{10}]$ to 1.12 for G-$[Mo_{132}]$. This effect can also reasonably be attributed to the diameter of IPyA, which increases with its charge. Concerning the charge matching between the IPyA and gelatin, Figure 2b depicts the evolution of the molar charge ratio (n^-/n^+) versus the charge density of IPyA. This last parameter can be evaluated by the quantity corresponding to the charge of IPyA divided by the number of metallic atoms of IPyA. In this figure, the data of POMs whose transition metals present a mean oxidation state between 5.5 and 6 are compared. Two behaviors can be clearly distinguished: for coacervates with IPyAs of low charge density (i.e., G-$[SiW_{12}]$ and for G-$[Mo_{132}]$), the charge matching between IPyA and gelatin is almost perfect, while for coacervates with IPyAs of higher charge density (i.e., G-$[BW_{12}]$, G-$[PW_{11}]$, and G-$[P_8W_{48}]$), the excess of negative charges of IPyA is compensated by the presence of countercations. Interestingly, although the positive and negative charges provided by IPyA and gelatin are equilibrated in G-$[Mo_3S_4]$, this coacervate contains a significant amount of sodium chloride, suggesting the influence of the ionic strength on the coacervation process, as already reported for protein/polysaccharide systems.[90] The influence of the charge density of IPyA on the molar charge ratio of coacervates is particularly remarkable in the Keggin POM-based hybrids. Although exhibiting the same IPyA/G molar ratio (**X** ≈ 9), the excess of negative charges of Keggin POM-based hybrids becomes increasingly important as the charge density of IPyA increases. By changing the charge of the POM from −4 to −6, the molar charge ratio increases by ∼40%. Concerning the coacervate G-$[P_8W_{48}]$, its global charge is counterbalanced by a large excess of cations, some of which are possibly encapsulated in the inner cavity of the $[H_{16}P_8W_{48}O_{184}]^{24-}$ macrocycle that exhibits strong chelating properties.

In order to determine the amount of gelatin triple helices of the prepared coacervates, differential scanning calorimetric (DSC) measurements were performed on coacervates. Indeed,

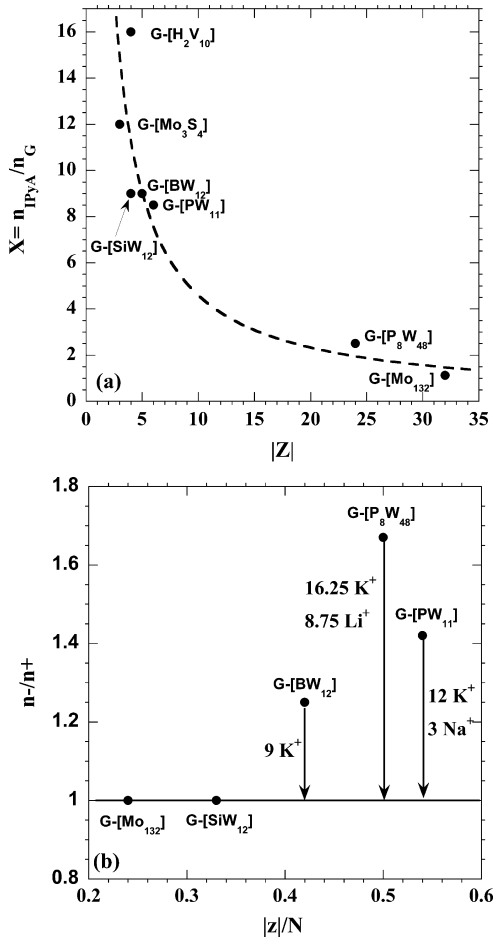

Figure 2. (a) Evolution of the IPyA/G molar ratio with the charge of the polyanion. The line corresponds to a fit of the data with a power law. (b) Evolution of the molar charge ratio (n^-/n^+) versus the charge density of the polyanion. n^- correspond to the amount of negative charges provided by the polyanion and n^+ corresponds to that of positive charges arising from gelatin. The charge density is evaluated by the quantity corresponding to the charge of the polyanion (Z) to their number of metallic centers (N).

when gelatin hydrogels are heated, the helix−coil transition occurs, during which the triple helix melts and progressively dissociates into the three randomly coiled peptide chain.[26] Two series of DSC experiments were performed on freshly prepared coacervates (hydrated samples; see Figure S12 in the SI) and coacervates aged for ∼24 h (dried samples). The $[V_{10}]$-G coacervate could not be investigated by DSC, because of a reduction of V^{5+} upon dehydration[70] that may alter the helix/coil ratio of gelatin. For comparison, we have also prepared pure gelatin coacervates upon ethanol addition ([gelatin] = 45.0 wt %, [H_2O] = 55.0 wt %). Figure S12c in the SI and Table 2 in the current work give the values of the melting enthalpy of samples.

For both series, the DSC thermograms of coacervates containing IPyA (Figure S12a in the SI) can be distinguished from pure gelatin coacervates by the presence of one or two thin endothermic peaks at temperatures of >120 °C. The enthalpy and temperatures characterizing these peaks vary in a reproducible manner from one IPyA to another, suggesting that these events are specific to the different IPyAs (see DSC thermograms of pure IPyAs in Figure S12b in the SI). At temperatures of <120 °C, extended endothermic peaks starting

from ~50 °C are observed for all the samples including pure gelatin coacervates. This contribution should result from water vaporization and gelatin triple helix melting, making precise determination of the amount of triple helices difficult. However, since IPyA–gelatin coacervates present similar water content (~40–50 wt %; see Table S5 in the SI) and their kinetics of drying is particularly slow during the first 10 min (see Figure S16 in the SI), it may be assumed that the heat of water vaporization is about the same for all the samples. Therefore, the enthalpy associated with this peak can be compared among the samples and will qualitatively reflect the amount of gelatin triple helices. As indicated in Table 2, since the enthalpy associated with the endothermic peak is similar for coacervates such as G-[BW_{12}], G-[PW_{11}], G-[SiW_{12}]), and G-[P_8W_{48}] (except for G-[Mo_{132}], which is slightly larger), the gelatin triple helix content is expected to be roughly similar for these coacervates, while that of G-[Mo_3S_4] may be significantly larger. In contrast for dried samples, the water vaporization does not overlap with the melting of gelatin triple helices. Compared to hydrated coacervates, higher melting enthalpies are obtained for all the coacervates, but one can derive the same trend concerning the relative amount of gelatin triple helices in the coacervates. Indeed, while the melting enthalpies are approximately the same for G-[BW_{12}], G-[PW_{11}], G-[SiW_{12}]), and G-[P_8W_{48}], that for G-[Mo_3S_4] is twice that of other coacervates. It is worth noting that the melting enthalpy values of G-[Mo_{132}] and pure gelatin coacervate on both hydrated and dried samples are intermediate between those of G-[BW_{12}], G-[PW_{11}], G-[SiW_{12}]), G-[P_8W_{48}], and G-[Mo_3S_4] (see Figure S12c in the SI).

SEM, EDX Experiments on IPyA–Gelatin Coacervates. The texture and the surface morphology of IPyA-G coacervates has been investigated by SEM-FEG. First, the surface of these coacervates has been observed by depositing the hybrid hydrogels on carbon substrates, followed by drying at room temperature. These materials exhibit generally a uniform and dense surface (see see panels (a1), (b1), (d1), and (e1) in Figure S14 in the SI), which is certainly imparted mainly by the biopolymer, as already reported.[70] The surface is also quite smooth, despite the presence of a few aggregates. The internal surface and texture of the IPyA-G coacervates has been characterized by SEM-FEG on fractured samples (see Figure S14 in the SI). The SEM images show clearly that the microstructure of these coacervates is composed of interconnected aggregates with quite a large distribution of diameters (on the nanometer and micrometer length scale), depending on the nature of coacervates. This observation is in full agreement with the previously reported characterization of multilayer gelatin–[$BW_{12}O_{40}$]$^{5-}$ films via atomic force microscopy (AFM).[85] Moreover, the presence of IPyA–gelatin aggregates is fully consistent with the coacervation process and the previous characterization of gelatin–[$H_{16}P_8W_{48}O_{184}$]$^{24-}$ semidiluted solution by combining small-angle neutron scattering (SANS) and static/dynamic light scattering.[61] According to these experiments, it was observed that diluted solution of gelatin and [$H_{16}P_8W_{48}O_{184}$]$^{24-}$ at 50 °C contains small, finite-sized aggregates ($R_{1,G} \approx 7.3$ nm) that possibly coexist with individual POMs ($R_{2,G} \approx 1.5$ nm).[61] Upon cooling the mixture at RT, and, thus, upon the gelatin triple helix renaturation, individual clusters are no longer detected via SANS while aggregates of a larger size ($R_{1,G} \approx 18$ nm) were evidenced, showing that an aggregation and growing process occurs. The distribution of IPyAs in coacervates is studied by recording SEM images with elemental mapping via EDX analysis. The elemental mapping on rectangular areas shown in Figure S15 in the SI demonstrates an excellent uniform distribution of metal (W, Mo) and heteroatom (S, P, Si, or B) elements. The relative atomic percentage of some elements are in agreement with the molecular structure of IPyAs. According to the complete characterization of IPyA-G hybrids, their structure can be described by the supramolecular assembly of IPyAs and gelatin (see Scheme 2). As reported for concentrated gelatin hydrogels,[26] bundles of gelatin triple helices are presumably present.

Scheme 2. Proposed Model of IPyA–Gelatin Coacervates ([$Mo_{132}O_{372}(CH_3COO)_{30}(H_2O)_{72}$]$^{42-}$ Is Chosen as a Typical Example)

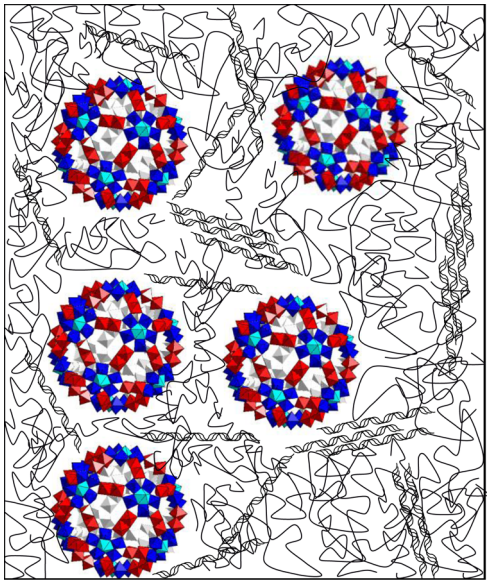

Tensile Tests until Failure of IPyA–Gelatin Coacervates. The mechanical properties of the undried IPyA–gelatin hybrids were investigated at large deformation by performing tensile tests until failure and tensile tests in cycling at different strain amplitudes. For that purpose, these samples were prepared similarly using the same procedure. Since aqueous gelatin hydrogels present particular weak mechanical properties, we have used the pure gelatin coacervate as a reference of unfilled gelatin coacervate. Quantitative measurements were obtained at RT by considering well-defined geometry test samples (Figure 1) cut to the required dimensions from homogeneous thick tablets prepared via a simple handling procedure taking advantage of the gelatin sol–gel transition (see the Experimental Section).

First of all, it was of primary importance to assess and control the drying kinetics of the different samples, which can depend strongly on the nature and composition of coacervates. Actually, we have observed that these coacervates evolve upon drying to glassy materials with a classical brittle failure, which is in complete agreement with that previously reported.[26,70] In particular, for the gelatin coacervate, we have observed that the Young's modulus (E) and σ_{break} increase notably while λ_{break} decreases as the drying rate increases (see Figure S17 in the SI), as previously reported.[70] This observation is presumably due to an increase in the glass-transition temperature (T_g) of gelatin with dehydration.[91,92]

Table 3. Average Mechanical Parameters of IPyA−Gelatin Hybrids at a Weight Loss of $\Delta m/m_0$ = 0.01 during Drying under Ambient Conditions (T = 23 °C, HR = 54%, 24 h)

coacervate	λ_{break}	σ_{break} (MPa)	E (MPa)	G (MPa)	E/G	mechanical behavior
gelatin	4.9 ± 0.7	0.7 ± 0.4	1.0 ± 0.3			plastic
G-[V_{10}]	8.0 ± 0.8	0.13 ± 0.06	0.05 ± 0.03	0.017 ± 0.005	3.0	elastomer
G-[Mo_3S_4]	6.8 ± 0.4	0.3 ± 0.1	0.09 ± 0.02	0.03 ± 0.01	3.0	elastomer
G-[PW_{11}]	7.3 ± 0.3	0.36 ± 0.08	0.08 ± 0.02	0.023 ± 0.005	3.5	elastomer
G-[BW_{12}]	10.6 ± 0.5	0.11 ± 0.07	0.065 ± 0.008			ductile (S-shape)
G-[P_8W_{48}]	11 ± 1	0.4 ± 0.1	0.10 ± 0.02			ductile (S-shape)
G-[SiW_{12}]	12 ± 1	0.4 ± 0.1	0.22 ± 0.04			ductile (plastic)
G-[Mo_{132}]	11.5 ± 0.7	0.9 ± 0.3	0.5 ± 0.1			ductile (plastic)

The weight loss of coacervates has been measured as a function of the aging time (see Figure S16 in the SI), showing different kinetics of drying, depending on the composition of coacervates. Note that the drying kinetics of IPyA−gelatin hybrids are slowed considerably, compared to that of pure gelatin coacervates, which can be imparted to the higher proportion of solvent present in the latter samples and to the more-volatile nature of ethanol. For all the IPyA−gelatin hybrids, the weight loss remains quite low before 2 h of aging. We typically performed the tensile measurements before 10 min of drying for which the weight loss $\Delta m/m_0$ is lower than 0.01 for all coacervates. Moreover, taking into account the very short duration of a typical tensile experiment ($t \approx 30$ s), we consider that the effects of drying are negligible during the course of our measurements. The average mechanical parameters determined from 10 different samples for the different types of coacervates are listed in Table 3 in the current paper. Figure 3 displays the Cauchy stress σ (which is defined

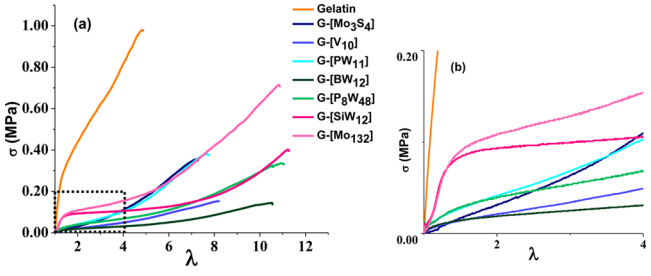

Figure 3. (a) Typical representation of a Cauchy stress ($\sigma = F/S_0$), as a function of stretch (λ) measured under the same experimental conditions (T = 23 °C, HR = 54%, $\Delta m/m_0$ = 0.01) for all the coacervates. (b) Enlarged view of the area in panel (a) represented by the dotted rectangle.

as $\sigma = F/S_0$, where F is the force measured at a given strain and S_0 is the initial section area of the sample), as a function of elongation (λ), for all the coacervates. Four different mechanical behaviors can be distinguished, depending on the nature of the coacervate.

The stress−elongation curve of gelatin is characterized by an initial linear elastic region, followed by a nonlinear behavior associated with a plastic deformation until failure for λ_{break} = 4.9 ± 0.7 and σ_{break} = 0.7 ± 0.4 MPa (see Figure S18a in the SI and Table 3 in the current work), as previously reported.[70] This plastic behavior is also revealed by the significant hysteresis of the loading−unloading cycles (see Figure S19 in the SI), indicating a poorly reversible deformation of this coacervate. The behavior of G-[V_{10}] coacervate (Figure S18c in the SI) characterized by an initial nonlinear part for $\lambda \leq 4.0$ and followed by an up-turn phenomenon until failure for λ_{break} = 8.0 ± 0.8 and σ_{break} = 0.13 ± 0.06 MPa (Table 3) is fully consistent with previously reported results.[70] Note that stress−elongation curves of similar shape were also obtained for the G-[Mo_3S_4] and G-[PW_{11}] coacervates (see Figures S18b−d in the SI) and are characteristic of rubberlike materials.[93] In order to determine the shear modulus (G) below the up-turn and to check if this behavior can be described by the neo-Hookean behavior relationship[94] ($\sigma = G(\lambda - \lambda^{-2})$), we have plotted σ as a function of ($\lambda - \lambda^{-2}$). As can been seen in the inset of Figures S18b−d in the SI, this basic model fits the experimental data in the λ range under study fairly well, confirming the rubbery character of G-[V_{10}], G-[Mo_3S_4], and G-[PW_{11}]. According to theses fits, values of the shear modulus (G) ranging from 0.017 ± 0.005 MPa to 0.03 ± 0.01 MPa (see Table 3) could be extracted. The Young's modulus (E) values are given by the slope of the linear part of the curves at very low deformation in the elastic regime. The E values (i.e., 0.05 ± 0.03 MPa < E < 0.09 ± 0.02 MPa) of G-[V_{10}], G-[Mo_3S_4] and G-[PW_{11}] are close to those found for unfilled elastomers.[93] Moreover, as given in Table 3 in the current paper, the E/G ratio is ∼3 for these coacervates, which is a typical value of unfilled elastomers.[93] At first glance, in comparison to previous coacervates (i.e., G-[V_{10}], G-[Mo_3S_4], and G-[PW_{11}]), the shape of the stress−elongation curves of G-[BW_{12}] and G-[P_8W_{48}] appears similar and composed of a nonlinear part, followed by an up-turn phenomenon, which is the signature of a rubbery behavior (see Figures S18e−g in the SI). However, their deformability is much larger (λ_{break} = 10.6 ± 0.5 for G-[BW_{12}] and λ_{break} = 11 ± 1 for G-[P_8W_{48}]). Moreover, it is not possible to extract the G modulus from the neo-Hookean model, since the E/G ratio deviates to 3, meaning that this model is not applicable for this type of material. Therefore, this complex behavior suggests that these materials can be described in a first approach only as ductile materials.[93] The shape of the stress−elongation curves of G-[Mo_{132}] and G-[SiW_{12}] (see Figures S18f−h in the SI) is completely different and composed of an initial linear part, followed by a plastic plateau, and finally by a strain hardening phenomenon until failure. This mechanical response can be ascribed to a ductile behavior involving a linear-elastic regime at small deformations, followed by a large plastic deformation.[93] Compared to other coacervates, the steep increase of the stress in the linear-elastic part of the curve is remarkable and explains peculiarly high E values. At the same time, these materials present a large deformability (λ_{break} = 12 ± 1 for G-[SiW_{12}] and λ_{break} = 11.5 ± 0.7 for G-[Mo_{132}]) and a relatively high Young's modulus (E = 0.22 ± 0.04 MPa for G-[SiW_{12}] and E = 0.5 ± 0.1 MPa for G-[Mo_{132}]), compared to the others coacervates. Furthermore, in order to assess the rubbery character of G-[Mo_3S_4] and G-[PW_{11}], we have studied the ability of these coacervates to

recover their initial shape by performing one loading−unloading cycle (until λ_{max}) followed by one uniaxial tensile measurement until failure (until λ_{break}). Similar experiments have been previously performed for G-[V_{10}].[70] Figures S20 and S21 in the SI show these cycling tests for G-[Mo_3S_4] and G-[PW_{11}] coacervates. For all these experiments, it appears that λ_{break} is only slightly dependent on the value of λ_{max} and, whatever the value of λ_{max}, when the second extension exceeds λ_{max}, the stress−elongation curve of these materials is almost identical to that reported for the monotonous uniaxial tensile test. For G-[Mo_3S_4], the hysteresis between the loading and unloading curve (Figure S20 in the SI) is almost absent, meaning that the deformation of G-[Mo_3S_4] is reversible, in agreement with the behavior of an unfilled elastomer. In contrast, for G-[PW_{11}] (Figure S21 in the SI), an hysteresis can be clearly distinguished, showing that the main fraction of the mechanical energy is dissipated during shape recovery. This irreversible component, which can be followed by the residual extension (permanent set),[95] seems to increase with λ_{max}. As previously reported for the G-[V_{10}] coacervate,[70] for $\lambda \leq \lambda_{max}$, one can observe a reduction in the stress when the second extension is applied, which is consistent with a softening effect. All these observations concerning G-[V_{10}], G-[Mo_3S_4], and G-[PW_{11}] are characteristic of rubberlike materials.

Comparison of the Mechanical Properties of IPyA−Gelatin Coacervates: Influence of the Charge, Size, and Molecular Structure of IPyA. Previous studies that involved the mechanical properties of aqueous gelatin hydrogels through the application of different deformations (shear deformation, compression, crack dynamic, etc.) have clearly pointed out that the synthetic and physicochemical parameters for the preparation of samples are strongly relevant for the control of their mechanical responses.[22−34] In the present work, the comparison of the mechanical behavior of these gelatin-based samples appears more straightforward, since the eight present coacervates have been prepared following the same chemical route and their mechanical properties were experimentally conducted using the same methodology. It is well-known that aqueous gelatin hydrogels exhibit very poor mechanical properties, characterized by a linear elastic behavior at low strain, followed by a nonlinear stress−elongation relationship before breaking at λ = 1.3−2.0.[96−100] As previously reported by some of us, simple gelatin coacervates exhibit the same plastic behavior, except that the Young's modulus (E) and the failure parameters (λ_{break} and σ_{break}) are significantly higher than those of gelatin hydrogels, demonstrating an enhancement of the stiffness of the material.[70] These results can be explained by the molecular structure of those gelatin compounds whose network is built by gelatin chains that are partially in a rigid crystalline triple helix state (cross-links) and partially in a random coil state (network bond). The balance between both conformations is directly linked to the gelatin concentration, since the gelatin triple helix content becomes more important as this concentration increases, as previously reported by Djabourov et al.[101] The relative triple helix/coil amount directly impacts the mechanical properties of gelatin, as previously experimentally evidenced through the measurement of Young's modulus of gelatin hydrogels that increase linearly with the gelatin concentration.[97] The influence of the gelatin random coils content on the extensibility of the gelatin-based materials can be interpreted according to the work of Bot et al.[97] Since the network bonds behave as anharmonic springs at large strain, the growth of the crystalline regions has the effect that the coils between two cross-links become shorter, thus decreasing the extensibility of gelatin chains upon deformation. Concerning the pure gelatin hydrogels and coacervates, a similar interpretation of their mechanical properties has been proposed according to their difference in gelatin concentration ([G] = 45 wt % for gelatin coacervates and [G] < 15 wt % for gelatin hydrogels).[70] Therefore, the high concentration of gelatin in simple coacervates gives rise to a significant increase of the Young's modulus and failure parameters (σ_{break} and λ_{break}), compared to those of gelatin hydrogels, and, consequently, to a higher stiffness. Different inorganic fillers, including clay minerals (sepiolite, montmorillonite) or silica, have been incorporated in gelatin hydrogels as reinforcing agents in order to enhance the mechanical properties of gelatin that are particularly critical for tissue engineering applications, such as bone scaffolds.[20−24,34−37] In contrast, to the best of our knowledge, the incorporation of polyoxometalate or inorganic polyanions into a gelatin matrix has not been previously reported so far. A comparison of the stress−elongation curves of these IPyA−gelatin composites is depicted in Figure 3. Compared to gelatin coacervate, the mechanical properties of these hybrid coacervates are significantly enhanced. First, these materials are much more extensible: G-[P_8W_{48}], G-[BW_{12}], G-[SiW_{12}], and G-[Mo_{132}] exhibit the highest elongation. It is interesting to note that some IPyA−gelatin coacervates with very different chemical compositions (i.e., G-[Mo_3S_4] and G-[PW_{11}]) exhibit similar mechanical behavior and, conversely, one can find a very different mechanical behavior for coacervates with structurally analogous polyoxometalates and similar IPyA/G ratios (**X** and **R**) (i.e., G-[BW_{12}] and G-[PW_{11}]). It is noteworthy that, depending on the nature of IPyA, three distinct mechanical behaviors can be clearly distinguished:

(i) G-[Mo_3S_4], G-[V_{10}], and G-[PW_{11}] show comparable extensibility ($\lambda_{break} \approx 7-8$), a E/G value of ∼3, and rather good reversibility in cycling experiments, which is consistent with the mechanical behavior of a unfilled elastomer;

(ii) in comparison, G-[P_8W_{48}] and G-[BW_{12}] can withstand higher elongation ($\lambda_{break} \approx 11$) and their mechanical behavior is characteristic of a ductile material; and

(iii) finally, G-[SiW_{12}] and G-[Mo_{132}] are also highly extensible materials but exhibit higher E values than other hybrid coacervates. These coacervates can be considered as ductile materials characterized by a large irreversible deformation.

Figure 4, as well as Figure S22 in the SI show a comparison of the mechanical parameters (E, σ_{break}, and λ_{break}) for all the coacervates. Except the particularly high E value for G-[Mo_{132}], it appears that λ_{break} is the most distinctive mechanical parameter that can be used to characterize and compare the mechanical properties of those coacervates. The evolution of λ_{break}, with weight ratios ($\mathbf{R}$ = wt $\%_{IPyA}$/wt $\%_G$) and molar ratios ($\mathbf{X} = n_{IPyA}/n_G$) as depicted in Figures 4c and 4d, shows the strong correlation between the composition of coacervates and their mechanical properties. It is noteworthy that the less-extensible coacervates of unfilled elastomer type (i.e., G-[Mo_3S_4] and G-[V_{10}]) are characterized by low $\mathbf{R}$ ratios (∼0.3−0.39) while the most extensible ones of ductile types present larger $\mathbf{R}$ values (0.55−0.81). It appears that the gelatin content has a significant impact on the extensibility of coacervates: the higher this gelatin content is, the lower their extensibility. As

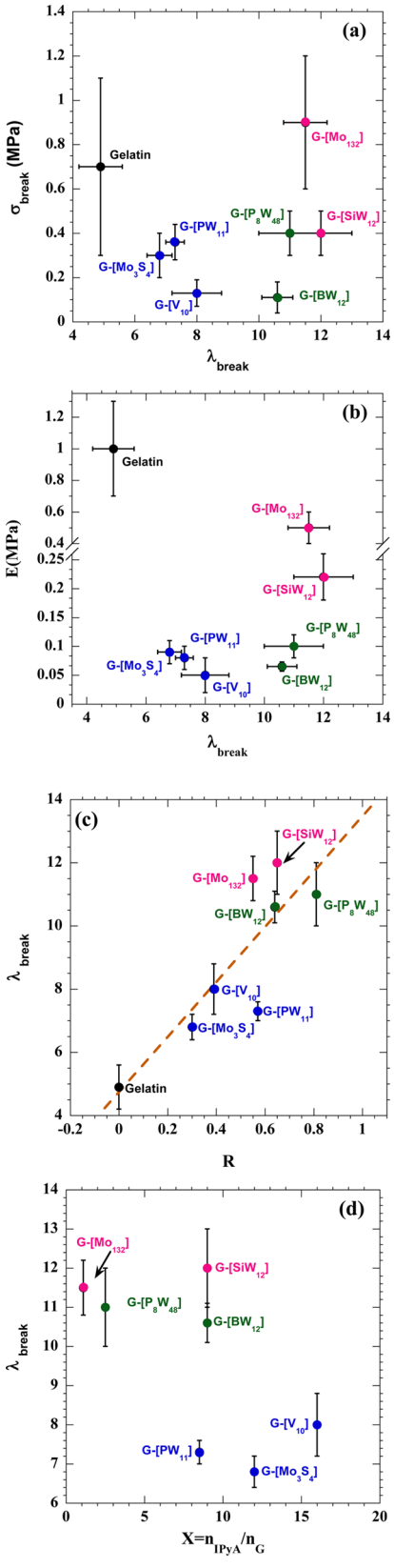

Figure 4. Comparison of the mechanical properties of gelatin–polyanion hybrids. Evolution of (a) σ_{break} and (b) the Young's modulus (E) versus λ_{break}. Evolution of λ_{break} as a function of (c) the weight ratio ($\mathbf{R}$ = wt $\%_{IPyA}$/wt $\%_G$ and (d) the molar ratio ($\mathbf{X} = n_{IPyA}/n_G$). The results of elastomers, ductile (S-shape) materials, and ductile (plastic) materials are represented by the colors blue, green, and pink, respectively.

reported previously, it seems that this gelatin content is directly related to the density of gelatin triple helices.[70,101] Moreover, DSC experiments on gelatin and IPyA–gelatin coacervates tend to confirm this assumption, since the amounts of gelatin triple helices in G-[Mo_3S_4] and pure gelatin coacervates are significantly higher than those of other coacervates (i.e., G-[BW_{12}], G-[PW_{11}], G-[SiW_{12}]), G-[P_8W_{48}], and G-[Mo_{132}]). Therefore, we may assume that the large extensibility of ductile-type coacervates may be partially explained by the low content of triple helices. Accordingly, the coil regions located between two cross-links may be longer and more stretched during deformation. Moreover, the large deformation of the most extensible coacervates (i.e., G-[P_8W_{48}], G-[BW_{12}], G-[SiW_{12}], and G-[Mo_{132}]) may be explained by the fact that the electrostatic interactions between gelatin chains are possibly screened by the inorganic polyanions, thus promoting a Gaussian conformation of gelatin chains and a strong degree of their entanglement. It may be assumed that the IPyAs are exerting multiple roles on the mechanical properties of coacervates. Figure 4d shows the strong dependence of λ_{break} with the molar ratio of $X = n_{IPyA}/n_G$. The extensibility of coacervates decreases as the amount of IPyA increases, in fair agreement with the role of IPyA as reinforcing fillers. The G-[Mo_3S_4] and G-[V_{10}] coacervates, which combine the highest molar amounts of IPyA and gelatin, present the lowest extensibility. Moreover, IPyAs are also expected to stabilize the crystalline regions of gelatin by preserving the reticulation of triple helices, according to our previous study of diluted decavanadate–gelatin solutions by rheology and microcalorimetry.[69] This work has clearly shown that the presence of decavanadate–gelatin cross-links may promote both a larger renaturation level of gelatin at the first stage of the cooling process and a higher thermal stability of triple helices. As clearly depicted in Figures 4c and 4d, the mechanical behavior of G-[PW_{11}] does not follow the same trend as the other coacervates, since its elongation is comparatively much lower than expected according to its weight and molar IPyA/G ratios. This observation is quite intriguing by taking into account the notably larger extensibility of coacervates embedding other Keggin-type POM (i.e., G-[SiW_{12}] and G-[BW_{12}]). Moreover, it is remarkable that all coacervates elaborated from Keggin polyanions present analogous stoichiometry, since the weight and molar IPyA/G values are quite close ($0.57 < \mathbf{R} < 0.65$ and $8.5 < \mathbf{X} < 9$). Moreover, DSC experiments have a tendency to show that the amount of gelatin triple helices is comparable in coacervates based on Keggin ions (i.e., G-[BW_{12}], G-[PW_{11}], and G-[SiW_{12}]). Therefore, the low extensibility of G-[PW_{11}] may not be only explained by its density of cross-links (gelatin triple helices and IPyA). These results suggest that the particular low extensibility of G-[PW_{11}] is certainly derived from the interactions of the polyoxometalate with gelatin through hydrogen bonds and/or electrostatic interactions. Accordingly, the ^{31}P MAS NMR experiments (see above) have shown that G-[PW_{11}] contains polyoxotungstates of different nuclearity with a main fraction of $[HPW_{11}O_{39}]^{6-}$, suggesting that this POM is particularly reactive in the presence of gelatin. These results suggest that stronger electrostatic interactions between $[HPW_{11}O_{39}]^{6-}$ and gelatin may occur and induce a notable strain hardening and a lower extensibility, compared to other Keggin-type POM–gelatin coacervates. Actually, one of the main differences between the Keggin-type POMs of this work is that $[HPW_{11}O_{39}]^{6-}$ is characterized by an anionic lined by oxo ligands with a strong nucleophilic

character. This interesting case of G-[PW_{11}] reveals that the mechanical properties of elastomers are strongly derived by the compatibility between inorganic fillers and polymer and their interfacial properties, as reported earlier on different materials.[3−7,15−18,22−24,34−40]

CONCLUSIONS

In this present article, a large family of bionanocomposites has been successfully prepared by a soft chemical approach that implies the assembly of inorganic polyanions and gelatin in aqueous solution. These biohybrid materials result from a complex coacervation process that could be induced by controlling the chemical procedure by which the components are brought together (pH, concentration, molar ratios). While the synthesis of bionanocomposites through a coacervation process has been mainly reported for biogenic phases (silica, clay minerals, etc.),[47−50,102] little attention has been paid to date to those involving inorganic polyanions or polyoxometalates as inorganic precursors. The advantage of using POM instead of small inorganic nanoparticles is related to the fact that these complexes are particularly well-defined, in terms of molecular structure, charge density, functionality, and size[53−57] and may be regarded as soluble models of metal oxide nanoparticles. Here, by selecting a large choice of inorganic polyanions of different nuclearity and charge, it was possible to finely tune the stoichiometry of the IPyA−gelatin coacervates, which is fixed experimentally by the charge matching between both components. We have shown that these bionanocomposites present enhanced mechanical properties, compared to pure gelatin samples. Moreover, it appears that these mechanical properties, which can be tuned by selecting the appropriate polyanion, are mainly governed by the content of gelatin triple helices and IPyA. By considering their structural and chemical properties, it seems that the IPyAs behave as reinforcing fillers and certainly exert some control over the nucleation and stabilization of triple helices. Because of cost-effectiveness, ease of preparation, and biocompatibility, especially for coacervates with a very low IPyA content, these bionanocomposites may present great potential as high barrier films and capsules. Moreover, in the biomedical field, the synthesis of gelatin hydrogels and blends for the development of drug carriers, wound dressings, and scaffolds for tissue engineering has gained great interest and the incorporation of organic and inorganic species is a key step to improving the texture/porosity, mechanical properties, and cell proliferation.[4,9−11,22,23] More importantly, this systematic investigation of mechanical properties of composites by varying the nature of the inorganic filler (charge, nuclearity, etc.) may provide a better fundamental understanding of the mechanical reinforcement of a biopolymer and, ultimately, useful guidance in the design of optimized polymer/metal oxide filler nanocomposites.

ASSOCIATED CONTENT

Supporting Information

Additional figures and tables; molecular structures of IPyAs; chemical composition; FTIR data and spectra; ^{11}B, ^{1}H, and ^{31}P solution NMR; ^{11}B and ^{31}P MAS NMR; DSC thermograms; curves of one uniaxial tensile measurement and loading−unloading cycles; and comparison of mechanical parameters. This material is available free of charge via the Internet at http://pubs.acs.org/.

AUTHOR INFORMATION

Corresponding Author

*Tel.: 33 1 39 25 43 73. Fax: 33 1 39 25 44 52. E-mail: nathalie.steunou@uvsq.fr.

Notes

The authors declare no competing financial interest.

ACKNOWLEDGMENTS

The authors would like to acknowledge Farid Nouar (ILV, Versailles) for the SEM/EDX experiments and Muriel Bouttemy (ILV, Versailles) for fruitful discussions.

REFERENCES

(1) Darder, M.; Aranda, P.; Ruiz-Hitzky, E. *Adv. Mater.* **2007**, *19*, 1309.

(2) Darder, M.; Aranda, P.; Ferrer, M. L.; Gutierrez, M. C.; del Monte, F.; Ruiz-Hitzky, E. *Adv. Mater.* **2011**, *23*, 5262.

(3) Bitinis, N.; Hernandez, M.; Verdejo, R.; Kenny, J. M.; Lopez-Manchado, M. A. *Adv. Mater.* **2011**, *23*, 5229.

(4) Liu, Q.; Jiang, L.; Shi, R.; Zhang, L. *Prog. Polym. Sci.* **2012**, *37*, 715.

(5) Liu, B.; Shangguan, Y.; Song, Y.; Zheng, Q. *J. Appl. Polym. Sci.* **2013**, 973.

(6) Amsden, B. *Soft Matter.* **2007**, *3*, 1335.

(7) Celina, M. C. *Polym. Degrad. Stab.* **2013**, *98*, 2419.

(8) Wang, R.; Yao, H.; Lei, W.; Zhou, X.; Zhang, L.; Hua, K.-C.; Kulig, J. *J. Appl. Polym. Sci.* **2013**, 1546.

(9) Bruggeman, J. P.; de Bruin, B.-J.; Bettinger, C. J.; Langer, R. *Biomaterials* **2008**, *29*, 4726.

(10) Buttafoco, L.; Kolkman, N. G.; Engbers-Buijtenhuijs, P.; Poot, A. A.; Dijkstra, P. J.; Vermes, I.; Feijen, J. *Biomaterials* **2006**, *27*, 724.

(11) Yang, J.; Webb, A. R.; Pickerill, S. J.; Hageman, G.; Ameer, G. A. *Biomaterials* **2006**, *27*, 1889.

(12) Yang, J.; Webb, A. R.; Ameer, G. A. *Adv. Mater.* **2004**, *16*, 511.

(13) Lee, K. Y.; Mooney, D. J. *Chem. Rev.* **2001**, *101*, 1869.

(14) Bokobza, L. *Macromol. Mater. Eng.* **2004**, *289*, 607.

(15) Jiao, J.; Sun, X.; Pinnavaia, T. J. *Adv. Funct. Mater.* **2008**, *18*, 1.

(16) Park, I.; Pinnavaia, T. J. *Adv. Funct. Mater.* **2007**, *17*, 2835.

(17) Das, A.; Jurk, R.; Stöckelhuber, K. W.; Engelhardt, T.; Fritzsche, J.; Klüppel, M.; Heinrich, G. *J. Macromol. Sci., Part A: Pure Appl. Chem.* **2008**, *45*, 144.

(18) Lopez-Manchado, M. A.; Valentın, J. L.; Carretero, J.; Barroso, F.; Arroyo, M. *Eur. Polym. J.* **2007**, *43*, 4143.

(19) Arroyo, M.; Lopez-Manchado, M. A.; Herrero, B. *Polymer* **2003**, *44*, 2447.

(20) Allouche, J.; Boissière, M.; Hélary, C.; Livage, J.; Coradin, T. *J. Mater. Chem.* **2006**, *16*, 3120.

(21) Coradin, T.; Marchal, A.; Abdoul-Aribi, N.; Livage, J. *Colloids Surf. B* **2005**, *44*, 191.

(22) Frydrych, M.; Wan, C.; Stengler, R.; O'Kelly, K. U.; Chen, B. *J. Mater. Chem.* **2011**, *21*, 9103.

(23) Mahony, O.; Tsigkou, O.; Ionescu, C.; Minelli, C.; Ling, L.; Hanly, R.; Smith, M. E.; Stevens, M. M.; Jones, J. R. *Adv. Funct. Mater.* **2010**, *20*, 3835.

(24) Qazvini, N. T.; Bolisetty, S.; Adamcik, J.; Mezzenga, R. *Biomacromolecules* **2012**, *13*, 2136.

(25) Podczeck, F.; Jones, B. E. *Pharmaceutical Capsules*; Pharmaceutical Press: Grayslake, IL, 2004.

(26) Coppola, M.; Djabourov, M.; Ferrand, M. *Polymer* **2012**, *53*, 1483.

(27) Martucci, J. F.; Accareddu, A. E. M.; Ruseckaite, R. A. *J. Mater. Sci.* **2012**, *47*, 3282.

(28) Moscato, S.; Mattii, L.; D'Alessandro, D.; Cascone, M. G.; Lazzeri, L.; Serino, L. P.; Dolfi, A.; Bernardini, N. *Micron* **2008**, *39*, 569.

(29) Thein-Han, W. W.; Saikhun, J.; Pholpramoo, C.; Misra, R. D. K.; Kitiyanant, Y. *Acta Biomater.* **2009**, *5*, 3453.

(30) Jiankang, H.; Dichen, L.; Yaxiong, L.; Bo, Y.; Bingheng, L.; Qin, L. *Polymer* **2007**, *48*, 4578.
(31) Kathuria, N.; Tripathi, A.; Kar, K. K.; Kumar, A. *Acta Biomater.* **2009**, *5*, 406.
(32) Li, H.; Wang, D. Q.; Chen, H. L.; Liu, B. L.; Gao, L. Z. *Macromol. Biosci.* **2003**, *3*, 720.
(33) Nabeta, M.; Sano, M. *Langmuir* **2005**, *21*, 1706.
(34) Fernandes, F. M.; Manjubala, I.; Ruiz-Hitzky, E. *Phys. Chem. Chem. Phys.* **2011**, *13*, 4901.
(35) Mu, C.; Li, X.; Zhao, Y.; Zhang, H.; Wang, L.; Li, D. *J. Appl. Polym. Sci.* **2013**, 3141.
(36) Liu, X.; Smith, L. A.; Hu, J.; Ma, P. X. *Biomaterials* **2009**, *30*, 2252.
(37) Landi, E.; Valentini, F.; Tampieri, A. *Acta Biomater.* **2008**, *4*, 1620.
(38) Kniep, R.; Simon, P. *Angew. Chem., Int. Ed.* **2008**, *47*, 1405.
(39) Yang, Z.; Jiang, Y.; Yu, L. X.; Wen, B.; Li, F.; Sun, S.; Hou, T. *J. Mater. Chem.* **2005**, *15*, 1807.
(40) Zheng, J. P.; Li, P.; Ma, Y. L.; Yao, K. D. *J. Appl. Polym. Sci.* **2002**, *86*, 1189.
(41) Veis, A. *Adv. Colloid Interface Sci.* **2011**, *167*, 2.
(42) Kizilay, E.; Kayitmazer, A. B.; Dubin, P. L. *Adv. Colloid Interface Sci.* **2011**, *167*, 24.
(43) Turgeon, S. L.; Schmitt, C.; Sanchez, C. *Curr. Opin. Colloid Interface Sci.* **2007**, *12*, 166.
(44) Luzzi, L. A.; Gerraughty, R. J. *J. Pharm. Sci.* **1967**, *56*, 634.
(45) Madan, P. L.; Madan, D. K.; Price, J. C. *J. Pharm. Sci.* **1976**, *65*, 1476.
(46) Cooper, C. L.; Dubin, P. L.; Kayitmazer, A. B.; Turksen, S. *Curr. Opin. Colloid Interface Sci.* **2005**, *10*, 52.
(47) Pawar, N.; Bohidar, H. B. *Adv. Colloid Interface Sci.* **2011**, *167*, 12.
(48) Berret, J.-F.; Schonbeck, N.; Gazeau, F.; El Kharrat, D.; Sandre, O.; Vacher, A.; Airiau, M. *J. Am. Chem. Soc.* **2006**, *128*, 1755.
(49) Toprak, M. S.; McKenna, B. J.; Mikhaylova, M.; Waite, J. H.; Stucky, G. D. *Adv. Mater.* **2007**, *19*, 1362.
(50) Fresnais, J.; Berret, J.-F.; Frka-Petesic, B.; Sandre, O.; Perzynski, R. *Adv. Mater.* **2008**, *20*, 3877.
(51) Cha, J. N.; Birkedal, H.; Euliss, L. E.; Bartl, M. H.; Wong, M. S.; Deming, T. J.; Stucky, G. D. *J. Am. Chem. Soc.* **2003**, *125*, 8285.
(52) Cha, J. N.; Bartl, M. H.; Wong, M. S.; Popitsch, A.; Deming, T. J.; Stucky, G. D. *Nano Lett.* **2003**, *3* (7), 907.
(53) *Chem. Soc. Rev.* **2012**, *41* (22), 7325 (Themed issue: Polyoxometalate Cluster Science).
(54) Dolbecq, A.; Dumas, E.; Mayer, C. R.; Mialane, P. *Chem. Rev.* **2010**, *110*, 6009.
(55) Kortz, U.; Müller, A.; Van Slageren, J.; Schnack, J.; Dalal, N. S.; Dressel, M. *Coord. Chem. Rev.* **2009**, *253*, 2315.
(56) Sokolov, M. N.; Adonin, S. A.; Abramov, P. A.; Mainichev, D. A.; Zakharchuk, N. F.; Fedin, V. P. *Chem. Commun.* **2012**, *48*, 6666.
(57) Sokolov, M. N.; Adonin, S. A.; Mainichev, D. A.; Sinkevich, P. L.; Vicent, C.; Kompankov, N. B.; Gushchin, A. L.; Nadolinny, V. A.; Fedin, V. P. *Inorg. Chem.* **2013**, *52*, 9675.
(58) Ashraf, S. M.; Kaleem, S. *Anal. Biochem.* **1995**, *230*, 68.
(59) Ball, V.; Barsukova-Stuckart, M.; Kortz, U. *Colloid Polym. Sci.* **2013**, *291*, 1219.
(60) Raj, G.; Swalus, C.; Guillet, A.; Devillers, M.; Nysten, B.; Gaigneaux, E. M. *Langmuir* **2013**, *29* (13), 4388.
(61) Carn, F.; Boue, F.; Djabourov, M.; Steunou, N.; Coradin, T.; Livage, J.; Floquet, S.; Cadot, E.; Buhler, E. *Soft Matter* **2012**, *8*, 2930.
(62) Li, H.; Qi, W.; Li, W.; Sun, H.; Bu, W.; Wu, L. *Adv. Mater.* **2005**, *17*, 2688.
(63) Ball, V.; Ringwald, C.; Bour, J.; Michel, M.; Al-Oweini, R.; Kortz, U. *J. Colloid Interface Sci.* **2013**, *409*, 166.
(64) Long, D.-L.; Tsunashima, R.; Cronin, L. *Angew. Chem., Int. Ed.* **2010**, *49*, 1736.
(65) Pradeep, C. P.; Misdrahi, M. F.; Li, F.-Y.; Zhang, J.; Xu, L.; Long, D.-L.; Liu, T.; Cronin, L. *Angew. Chem., Int. Ed.* **2009**, *48*, 8309.
(66) Bu, W.; Uchida, S.; Mizuno, N. *Angew. Chem., Int. Ed.* **2009**, *48*, 8281.
(67) de Viguerie, L.; Mouret, A.; Brau, H.-P.; Nardello-Rataj, V.; Proust, A.; Bauduin, P. *CrystEngComm* **2012**, *14*, 8446.
(68) Carn, F.; Steunou, N.; Djabourov, M.; Coradin, T.; Ribot, F.; Livage, J. *Soft Matter* **2008**, *4*, 735.
(69) Carn, F.; Djabourov, M.; Coradin, T.; Livage, J.; Steunou, N. *J. Phys. Chem. B* **2008**, *112*, 12596.
(70) Carn, F.; Durupthy, O.; Fayolle, B.; Coradin, T.; Mosser, G.; Schmutz, M.; Maquet, J.; Livage, J.; Steunou, N. *Chem. Mater.* **2010**, *22*, 398.
(71) Sorribes, I.; Wienhöfer, G.; Vicent, C.; Junge, K.; Llusar, R.; Beller, M. *Angew. Chem., Int. Ed.* **2012**, *51*, 7794.
(72) Sorribes, I.; Llusar, R.; Vicent, C. *Eur. J. Inorg. Chem.* **2013**, *9*, 1418.
(73) Rocchicioli-Deltcheff, C.; Fournier, M.; Franck, R.; Thouvenot, R. *Inorg. Chem.* **1983**, *22*, 207.
(74) Souchay, P. *Ions Minéraux Condensés*; Masson et Cie: Paris, 1969.
(75) Contant, R. *Can. J. Chem.* **1987**, *65*, 568.
(76) Durupthy, O.; Steunou, N.; Coradin, T.; Maquet, J.; Bonhomme, C.; Livage, J. *J. Mater. Chem.* **2005**, *15*, 1090.
(77) Bouhedja, L.; Steunou, N.; Maquet, J.; Livage, J. *J. Solid State Chem.* **2001**, *162*, 315.
(78) Contant, R.; Tézé, A. *Inorg. Chem.* **1985**, *24*, 4610.
(79) Shibahara, T.; Yamasaki, M.; Sakane, G.; Minami, K.; Yabuki, T.; Ichimura, A. *Inorg. Chem.* **1992**, *31*, 640.
(80) Müller, A.; Krickemeyer, E.; Bögge, H.; Schmidtmann, M.; Peters, F. *Angew. Chem., Int. Ed.* **1998**, *37*, 3360.
(81) Fung, B. M.; Khitrin, A. K.; Ermolaev, K. *J. Magn. Reson.* **2000**, *142*, 97.
(82) Massiot, D.; Fayon, F.; Capron, M.; King, I.; Le Calvé, S.; Alonso, B.; Durand, J. O.; Bujoli, B.; Gan, Z.; Hoatson, G. *Magn. Reson. Chem.* **2002**, *40*, 70.
(83) Hohwy, M.; Jakobsen, H. J.; Eden, M.; Levitt, M. H.; Nielsen, N. C. *J. Chem. Phys.* **1998**, *108*, 2686.
(84) States, D.; Haberkorn, R.; Ruben, R. *J. Magn. Reson.* **1982**, *48*, 286.
(85) Khadro, B.; Baroudi, I.; Goncalves, A.-M.; Berini, B.; Pegot, B.; Nouar, F.; Ha Le, T. N.; Ribot, F.; Gervais, C.; Carn, F.; Cadot, E.; Mousty, C.; Simonnet-Jégat, C.; Steunou, N. *J. Mater. Chem. A* **2014**, *2*, 9208.
(86) Tézé, A.; Hervé, G.; Finke, R. G.; Lyon, D. K. *Inorganic Syntheses*, Vol. *27*; John Wiley & Sons: New York, 1990; p 85.
(87) Massart, R.; Contant, R.; Fruchart, J.-M.; Ciabrini, J.-P.; Fournier, M. *Inorg. Chem.* **1977**, *16*, 2916.
(88) Duval, S.; Dumur, F.; Guénée, L.; Marrot, J.; Simonnet-Jégat, C.; Cadot, E. *Eur. J. Inorg. Chem.* **2013**, 1149.
(89) Uchida, S.; Inumaru, K.; Misono, M. *J. Phys. Chem. B* **2000**, *104*, 8108.
(90) Schmitt, C.; Turgeon, S. L. *Adv. Colloid Interface Sci.* **2011**, *167*, 63.
(91) Coppola, M.; Djabourov, M.; Ferrand, M. *Macromol. Symp.* **2008**, *273*, 56.
(92) Yakimets, I.; Wellner, N.; Smith, A. C.; Wilson, R. H.; Farhat, I.; Mitchell, J. *Polymer* **2005**, *46*, 12577.
(93) Treloar, L. R. G. *The Physics of Rubber Elasticity*; Clarendon Press: Oxford, U.K., 1975.
(94) Flory, P. J. *Principles of Polymer Chemistry*; Cornell University Press: Ithaca, NY, 1953.
(95) Diani, J.; Fayolle, B.; Gilormini, P. *Eur. Polym. J.* **2009**, *45*, 601.
(96) Groot, R. D.; Bot, A.; Agterof, W. G. M. *J. Chem. Phys.* **1996**, *104*, 9202.
(97) Bot, A.; Van Amerongen, I. A.; Groot, R. D.; Hoekstra, L. L.; Agterof, W. G. M. *Polym. Gels Networks* **1996**, *4*, 189.
(98) Baumberger, T.; Caroli, C.; Martina, D. *Eur. Phys. J. E: Soft Matter Biol. Phys.* **2006**, *21*, 81.
(99) Baumberger, T.; Caroli, C.; Martina, D. *Nat. Mater.* **2006**, *5*, 552.

(100) Wilking, J. N.; Mason, T. G. *Phys. Rev. E* **2008**, *77*, 055101.
(101) Djabourov, M.; Leblond, J.; Papon, P. *J. Phys. (Paris)* **1988**, *49*, 319.
(102) Amali, A. J.; Singh, S.; Rangaraj, N.; Patra, D.; Rana, R. K. *Chem. Commun.* **2012**, *48*, 856.